ACS OMEGA

Article

Cite This: ACS Omega 2018, 3, 2340−2350

Enzyme-Free Immunoassay Using Silver Nanoparticles for Detection of Gliadin at Ultralow Concentrations

Pablo. A. Mercadal,[†] Juan C. Fraire,[†] Ruben D. Motrich,[‡] and Eduardo A. Coronado*[,†]

[†]INFIQC-CONICET, Centro Láser de Ciencias Moleculares, Departamento de Fisicoquímica, and [‡]CIBICI-CONICET, Departamento de Bioquímica Clínica, Facultad de Ciencias Químicas, Universidad Nacional de Córdoba, Córdoba X5000HUA, Argentina

Supporting Information

ABSTRACT: Determination of biomarkers in clinical or food samples is of crucial importance for monitoring, prevention, and care of public health. The standard procedure used for this purpose is the enzyme-linked immunosorbent assay (ELISA), which makes use of the specific antibody−antigen biorecognition and the catalytic effect of the enzymes. One of the main shortcomings of this technique is the use of enzymes that often present low chemical and thermal stabilities compared to other chemicals. Other drawbacks include the nonspecific binding process that could lead to false-positive results, the use of relatively large amounts of the sample, and the number of time-consuming steps involved. Recently, an enzyme-free and ultrasensitive analytical method for antigen detection denoted as intensity depletion immunolinked assay (IDILA) has been proposed by our laboratory. The assay is based on the inhibition to form Ag nanosphere dimers linked by a specific antibody in the presence of the corresponding antigen. In this work, we go a step further demonstrating how the performance of this method could be improved by using silver nanoparticles (Ag NPs) of different diameters (58 and 78 nm). The experiments are performed for detecting gliadin, an antigen of utmost importance in celiac disease, and the results are compared with ELISA, the standard technique homologated by the Food Codex Alimentarius. It is found that the IDILA assay could be around 1000 or 10 000 times more sensitive than ELISA, also having lower limits of detection, depending on the conditions explored (fraction of dimers and Ag NP diameter). Using the appropriate conditions, the IDILA assay is shown to be able to detect femtomolar concentrations of the antigen, besides being robust, reliable, cheap, rapid (around 2 h), and of easy implementation using the standard equipment and biomolecular reagents used for the ELISA assay.

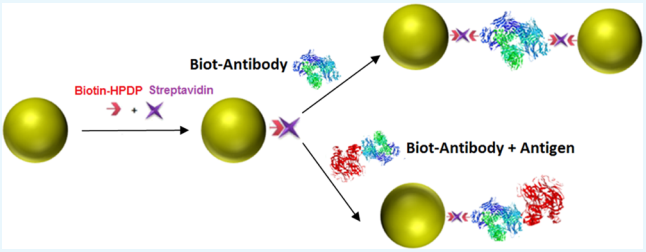

INTRODUCTION

Gluten is a set of proteins present in the flour of cereals such as wheat, barley, rye, oats, and their hybrid species.[1] This protein complex is composed of prolamin and glutenin. Gliadin is a type of prolamin present in the grain of wheat and is the protein responsible for causing celiac disease (CD).[2] CD is an immune-mediated enteropathy triggered by the ingestion of gluten in genetically susceptible individuals and represents a unique example of an immune-mediated disease for which early serologic diagnosis and dietary treatment can prevent severe and sometimes life-threatening complications. The prevalence of CD in different parts of the world has been estimated to be around 0.5−1%. In addition, the population bearing diabetes or autoimmune disorders or relatives of CD individuals have even higher risk for CD development.[3,4]

Therefore, the development of a methodology that allows the detection of gluten in a fast and specific sensitive way is a topic of great importance in food science for its implications in health care. Currently, the content of gliadin in food is determined by the well-known enzyme-linked immunosorbent assay (ELISA), a methodology that uses the basic immunology concept of antigen binding to its specific antibody.[5] In ELISA, the antigen in the fluid phase is immobilized, usually in 96-well plates, to a specific antibody, which is itself subsequently detected by a secondary, enzyme-coupled antibody that yields a visible color change or fluorescence, indicating the presence of the antigen.[6] There are however, several drawbacks associated with ELISA such as the use of enzymes whose chemical and physical stabilities are relatively low compared with other chemicals and the occurrence of nonspecific binding events to the plate, which could lead to false-positive results. Another issue is that the assay normally requires the use of large amounts of reagents and various washing steps.[7,8]

Considering the abovementioned shortcomings of the ELISA assay, the development of enzyme-free analytical assays that surmounts these limitations, specifically capable of rapid and specific antigen quantification, with improved stability, using smaller sample amounts, and with no false positives has become necessary. In recent years, continuous effort has been devoted to the development of reliable and robust enzyme-free

Received: November 22, 2017
Accepted: February 9, 2018
Published: February 27, 2018

DOI: 10.1021/acsomega.7b01840
ACS Omega 2018, 3, 2340−2350

detection methods. In fact, various advanced techniques, such as surface plasmon resonance, electrochemical, quartz crystal microbalance, and optical analyses have been applied for the detection and quantification of biomarkers based on different respective signal generation principles.[9,10] Nanoparticle (NP)-based trials have demonstrated to have the potential for detecting events and processes with unprecedented levels of sensitivity, location, and stability.[11−18] The high biocompatibility of these NPs, including metal NPs, carbon nanomaterials, metal oxide nanostructures, and semiconductor nanocrystals, has been successfully used for the development of qualitative and quantitative detection assays for several biomarkers based on their physical and chemical properties.[9,19,20] For instance, Yu et al. have recently designed MeLISA, an enzyme-free and metal-linked immunosorbent assay for the detection of ultralow concentrations of disease biomarkers, such as α-fetoprotein, prostatic specific antigen, and C-reactive protein. This method exhibits approximately 2 magnitudes higher sensitivity and is 4 times faster for a chromogenic reaction than ELISA. In MeLISA, the secondary or detection antibody is coupled to Ag NPs, which in the presence of H_2O_2 dissolves to produce millions of Ag^+ ions that are further converted into an amplified color signal by inducing the aggregation of alkyne-functionalized Au NPs[9] or by turning on the ultrasensitive silver ion fluorescence probe 3′,6′-bis(diethylamino)-2-(2-iodoethyl)-spiro[isoindoline-1,9′-xanthen]-3-one.[19]

In particular, because of their extreme sensitivity to the chemical environment, the optical properties of noble metal NPs are now widely used for the development of ultrasensitive molecular detection platforms.[18] This sensitivity is due to the so-called localized surface plasmon resonance (LSPR), the elementary quantum quasi-particle corresponding to the oscillation of the conduction electrons of the metal when illuminated by electromagnetic radiation. The LSPR can be tuned just by changing the geometrical parameters, such as the size, shape, dielectric environment, and particle−particle spacing. In addition, it could give rise to highly localized and enhanced electromagnetic fields, which is the basis for the so-called enhanced spectroscopy techniques such as surface-enhanced Raman spectroscopy, tip-enhanced Raman spectroscopy, and metal-enhanced fluorescence as well as optical imaging well below the diffraction limit of light.[21−26] Because of the abovementioned properties, a wide range of applications are having exponential growth in both basic and applied sciences, as for example, the design of ultrasensitive optical nanosensors and subdiffraction optical imaging techniques.[27−31] All of these developments are a very active area of research denoted as Plasmonics.[32−34]

Very importantly, the optical properties of noble metal NPs in combination with their surface properties are suitable for developing several functionalization strategies involving biomolecules that could be specific linkers and also biorecognition agents that are able to preferentially interact with target molecules.[35−37] The possibility of generating dimers of silver NPs linked by a specific antibody by stoichiometric control of the functionalization and to inhibit the dimer formation in the presence of the corresponding antigen has led us recently to propose a new and powerful analytical method, denoted as IDILA (intensity depletion immunolinked assay). The optical detection is possible because of the differences between the extinction cross-sections of two isolated monomers compared with one dimer and the different fraction of dimers produced at different antigen concentrations.[37]

In our early work, the capabilities of the method to detect ultralow concentrations of cytokines (biomarkers involved in the diagnosis and prognosis of chronic inflammatory diseases) were shown. The aim of the present work is several folds: first, to further investigate the general capabilities of IDILA to other antigens of importance in ood science, such as gliadin. Second, to understand the role played by the fraction of Ag NP dimers formed using Ag NPs of two different diameters upon its sensitivity and detection limits as well as the theoretical basis of the method in a more rigorous way.[37] For such a purpose, we have performed experiments as well as theoretical simulations with 58 and 78 nm diameter Ag NPs to explore the capabilities of the IDILA method to quantify ultralow concentrations of gliadin at different Ag NP sizes. Another important question that arises is the role played by the fraction of dimers (formed after the addition of a given amount of the antibody at a given time, in the absence of the antigen) on the sensitivity of the method. To answer this issue, we have also tested the method at two quite different fractions of dimers formed after the addition of a given amount of the antibody. Finally, we demonstrate the high potential of this method to detect ultralow concentrations of gliadin in real samples of food, using samples that are supposed to be gluten-free (corn starch and corn flour), where the standard ELISA fails, particularly for corn starch.

RESULTS AND DISCUSSION

NP Functionalization. The Ag NPs were functionalized in a 1:1:1 molar ratio with streptavidin (STV) and biotin (Biot). This chemical process was performed just by the addition of biotin HPDP simultaneously with the STV protein to reach the same concentration as that of the Ag NPs (calculated from the peak intensity of the extinction spectra using Beer's law and with the calculated extinction cross-section corresponding to each NP diameter). The STV−Biot combination was used because of the high kinetic and thermodynamic interaction constant of the STV−Biot complex which avoids the prior chemisorption of biotin molecules on the surface of Ag NPs that could lead to the formation of undesired aggregates.[27] The reaction using biotin HPDP leads to Ag NPs functionalized with biotin (due to its SH moiety) and mercapto-pyridine-2 thione. It should be noticed that although the pyridine-2-thione molecule will also bind to the surface of the Ag NPs, the presence of this molecule on its surface does not cause any difficulty. This is so because the presence of this molecule neither inhibits the surface functionalization with biotin (through its SH group) nor the interaction of biotin with STV and the subsequent specific antibody binding events with the antigen[28] (see Figure S1 in the Supporting Information).

The biotin (SH) covalently bound to the Ag NPs will interact strongly with STV, leaving the surface of the NP modified with the Biot−STV complex, with one of the sites bound to biotin and leaving three sites available for interacting with any biotinylated molecule. The addition of a biotinylated antibody will in this way interact with one of this STV sites. Then, if another Biot−STV-functionalized NP (free of antibody) approaches, a dimeric structure sandwiched by the biotinylated antibody will be produced.[35−37]

Because of the simultaneous addition of STV and biotin to the Ag NP colloidal dispersion and the strict stoichiometric control, the stability of the Biot−STV-functionalized colloidal dispersion is very high (see Figure S2A,B). The extinction spectra remain almost the same up to a time of 20 min with any

DOI: 10.1021/acsomega.7b01840
ACS Omega 2018, 3, 2340−2350

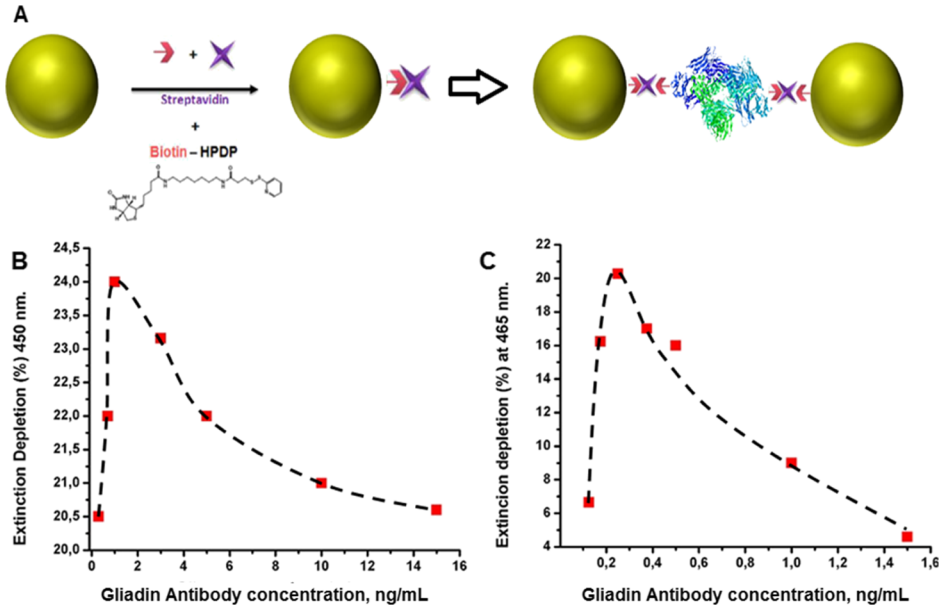

Figure 1. (A) Scheme of the Ag NPs biotin−STV interaction and the subsequent formation of dimeric structures in the presence of IgG Biot anti-gliadin. (B) Variation of the intensity of the extinction spectrum of Ag NPs (58 nm diameter) taken at a wavelength of 450 nm for different concentrations of gliadin IgG Biot. (C) Variation of the intensity of the extinction spectrum of Ag NPs (78 nm diameter) taken at a wavelength of 465 nm for different concentrations of gliadin IgG Biot.

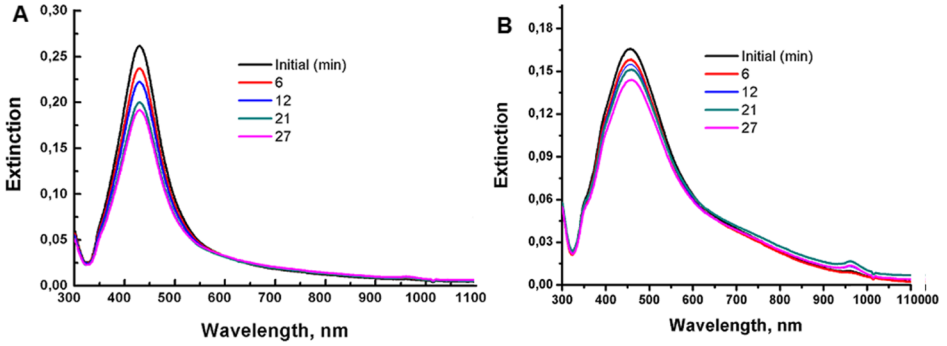

Figure 2. Evolution of the extinction spectra for two different average diameter colloidal dispersion Ag NPs in the presence of 1 ng/mL gliadin IgG Biot. (A) 58 nm diameter Ag NPs and (B) 78 nm diameter Ag NPs.

signature of NP aggregation [see transmission electron microscopy (TEM) images, Figure S3].

Influence of Ag NP Size and IgG-Biot Concentration on the Fraction of Dimers Formed. Once the NPs were functionalized, the next step consisted in forming controlled agglomerates (dimers) in the presence of the specific biotinylated antibody for gliadin (Figure 1A). The degree of dimerization will be spectrally reflected by the degree of depletion of the extinction intensity (see the theoretical discussion below). For a given experimental condition, as the intensity decreases, more dimers are formed.

To address the influence of the concentration of the IgG biotinylated anti-gliadin antibody (IgG-Biot) and the role played by the Ag NP size on the degree of dimerization, a set of experiments for 58 and 78 nm Ag NPs varying the antibody concentration were performed. All these experiments were carried out on a quartz cuvette using 0.5 mL of the 58 and 78 nm Ag NP colloidal dispersions previously functionalized with STV−Biot and different IgG-Biot concentrations supplemented with 5% bovine serum albumin (BSA) and phosphate-buffered saline (PBS) to complete a final volume of 1 mL. The extinction spectra were measured in the 300−1100 nm wavelength range.

For these series of experiments, the depletion of the intensity of extinction $E_{(D)}$ was calculated as $E_{(t)}/E_{(0)}$, where $E_{(t)}$ is the peak intensity of the extinction spectra at a given time (t) after adding a given amount of IgG-Biot and $E_{(0)}$ is the initial peak extinction intensity.

Figure 1 shows the variation of $E_{(D)}$ as a function of the gliadin antibody concentration for the two Ag NP diameters analyzed in the present work. The intensities were measured after 27 min, a time point after which no change of extinction was observed, that is, the spectra remain the same. The behavior for both Ag NP diameters is qualitatively the same. As the IgG-Biot concentration increases, $E_{(D)}$ begins to increase, then it reaches a maximum, and finally it decreases. The growing part of the curve indicates that the fraction of dimers formed is larger as the concentration of IgG-Biot increases; the maximum corresponds to the IgG-Biot concentration, which produces the highest fraction of dimers. The antigen concentrations where dimer formation is more favored are 1 and 0.25 ng/mL for the experiments performed using 58 nm (Figure 1B) and 78 nm (Figure 1C) Ag NPs, respectively. In

DOI: 10.1021/acsomega.7b01840
ACS Omega 2018, 3, 2340−2350

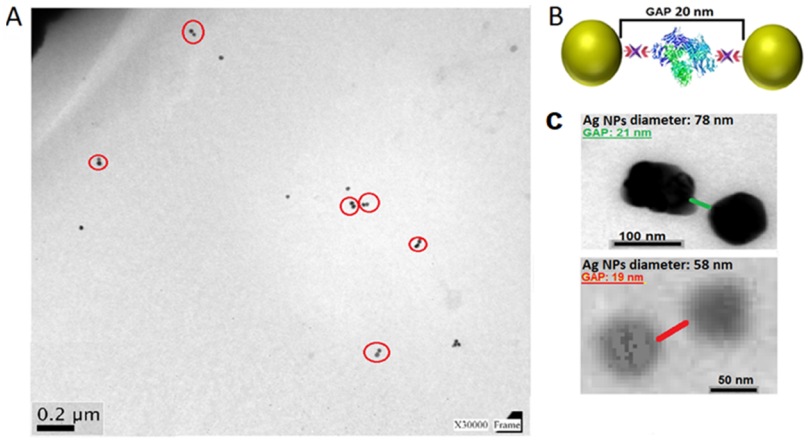

Figure 3. (A) TEM image of Ag NPs after 30 min of aggregation of 1 ng/mL gliadin IgG Biot, where it is evident that the presence of dimeric structures predominates over other nanostructures. (B) Interparticle distance estimation for the Ag NP dimer formed by the "sandwich" biotin−STV IgG Biot STV−biotin. (C) TEM images of some representative Ag NP dimers formed after 30 min of adding 1 ng/mL IgG Biot anti-gliadin for two different average diameter Ag NPs.

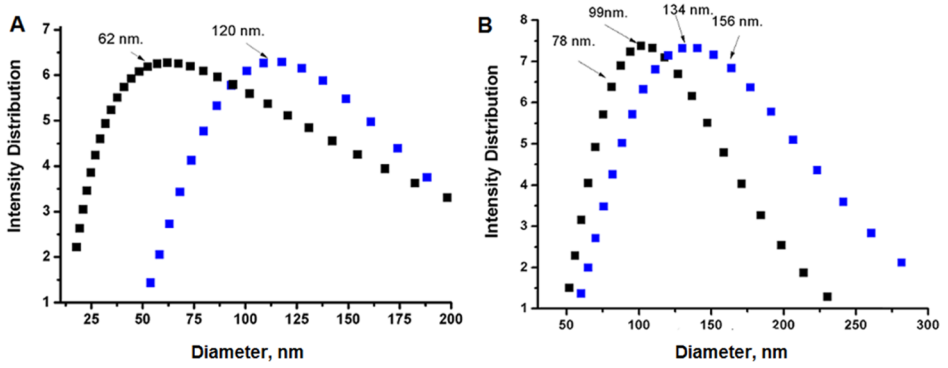

Figure 4. DLS distributions before (black symbols) and after (blue symbols) adding 1 ng/mL IgG Biot to Ag NP colloidal dispersions of different average sizes. (A) Average Ag NP diameter 58 nm and (B) average Ag NP diameter 78 nm.

both cases, the fraction of dimers formed can be estimated (as it will be discussed later) by electrodynamics calculations. The calculations show that in both cases, the fraction of dimers formed is almost the same (around 0.9). The antibody concentration needed to achieve the same degree of dimerization is 4 times larger for the colloidal dispersion that is 4 times more concentrated (58 nm Ag NPs). Therefore, it seems that the NP size has no effect on the degree of dimerization.

After the antibody concentration where the maximum extinction depletion is reached, the fraction of dimers formed decreases until reaching a value where the concentration of IgG-Biot is so high that under these conditions, most of the available binding sites of the STV molecules on the surface of each NP are occupied by individual IgG-Biot molecules inhibiting the dimer formation.

Dimerization Process at a Constant Antibody Concentration. The kinetics of dimerization for the same antibody concentration (1 ng/mL of IgG-Biot) was followed for both NP diameters for 27 min. The results of these experiments are shown in Figure 2A,B. For both NP sizes, the decrease in extinction evidences the formation of dimers, and for this antibody concentration, the depletion, $E_{(D)}$, after 27 min is 24 and 9% for 58 nm (Figure 2A) and 78 nm Ag NPs (Figure 2B), respectively. This result should indicate that the dimer formation using 1 ng/mL gliadin antibody is more favored for 58 nm than for 78 nm diameter Ag NPs, a result that is in good agreement with what has been shown in the previous section.

The morphological characterization of the structures formed at 27 min was performed by TEM using a diluted aliquot of the colloidal dispersion in such a way to avoid any in situ aggregation processes that could be generated on the grid during evaporation and diffusion of the aggregates. Some representative TEM images for both NP sizes evidenced the formation of mainly Ag NP dimers, with a small fraction of isolated Ag NPs (see Figure 3A).

Figure 3 depicts the magnified TEM images of the dimers, with a 20 nm average interparticle distance (gap) (Figure 3C), which is in excellent agreement with the distance that can be estimated from the size of the molecules linking the Ag NP dimers (Figure 3B). The "molecular bridge" formed by the molecules biotin−STV−Biot-IgG−STV−biotin gives an interparticle distance value of around 20 nm. A set of additional TEM images are also shown in Figure S5 panels A and B.

Dynamic light scattering (DLS) measurements also validate the formation of NP aggregates. The distribution of DLS intensities of the 58 and 78 nm Ag NPs colloidal dispersions before the addition of the antibody (black dotted lines in Figure 4A,B) shows a maximum for an average hydrodynamic diameter at around 62 and 99 nm, respectively. The DLS distribution (after 27 min of adding the antibody) is clearly shifted to larger sizes (blue dotted lines, Figure 4A,B), having a maximum at 120 and 134 nm for 58 and 78 nm Ag NPs,

DOI: 10.1021/acsomega.7b01840
ACS Omega 2018, 3, 2340−2350

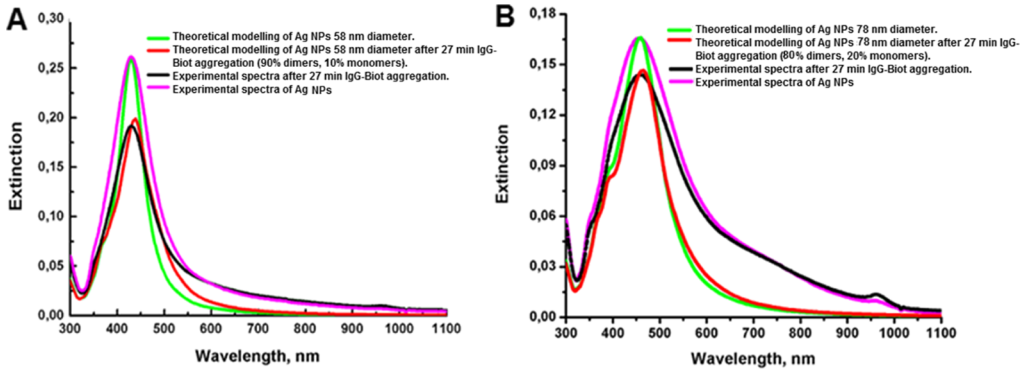

Figure 5. Comparison between the experimental (pink and black lines) and simulated (green and red lines) extinction spectra before and after 27 min of adding 1 ng/mL IgG Biot for two different diameter-functionalized Ag colloidal dispersions. The fraction of dimers f_d was estimated using eq 2. (A) 58 nm Ag NPs with f_d = 0.9 and (B) 78 nm Ag NPs with f_d = 0.2.

respectively. This observation qualitatively indicates the formation of structures of larger sizes (dimers).

Comparison between Experiments and Theoretical Simulations. Another more rigorous way of corroborating the observed experimental data is through electrodynamics modeling using the Mie theory (for isolated Ag NPs) and the generalized Mie theory for multiple particles (for Ag dimers).

In all calculations, we considered average Ag NP diameters of 58 and 78 nm. For the calculations of the effective cross-sections of the dimers, an interparticle distance of 20 nm was considered.

The first issue that arises is to understand why the formation of dimers is spectrally evidenced as a decrease in the intensity of the extinction spectrum.[37] The theoretical simulation of the extinction spectra using the Mie theory for Ag monomers of 58 and 78 nm (see Figure S6) shows that the extinction cross-section σ_{ext} for the smaller and larger Ag NPs are $\sigma_{ext} = 2.88 \times 10^{-10}$ cm^2 and $\sigma_{ext} = 4.43 \times 10^{-10}$ cm^2, respectively. The average extinction cross-section for the dimers formed for each NP size are $\sigma_{ext} = 4.35 \times 10^{-10}$ cm^2 for 58 nm Ag NP dimers and $\sigma_{ext} = 7.14 \times 10^{-10}$ cm^2 for the dimers formed from 78 nm Ag NPs (see Figure S6). The sum of the extinction cross-sections of the two isolated monomers (separated at very large distances) is $\sigma_{ext} = 5.76 \times 10^{-10}$ cm^2 (red line in Figure S6A) and $\sigma_{ext} = 8.86 \times 10^{-10}$ cm^2 for the 58 and 78 nm diameter Ag NPs (red line in Figure S6B), respectively. The main factors that explain why the formation of dimer structures produces a depletion of the extinction intensity are the lower values of the extinction cross-section of each dimer compared with the cross-section of the corresponding monomers and the negligible shift of the extinction spectra of the dimer relative to the corresponding monomer (because of the small plasmon coupling due to the relative large gap between the Ag NPs). Another factor is that the final concentration of NPs is smaller (in the limit where all monomers form dimers, the concentration of dimers should be one-half the concentration of monomers).

As it can be appreciated in Figure 5, there is a very good agreement between the experimental (pink line) and the simulated extinction spectra for the colloidal dispersion of Ag NPs (without the addition of IgG-Biot) for both NP diameters. The concentration of NPs was determined from Beer's law from the peak intensity of the experimental extinction spectra $I_{(E)}$ and using the values of the theoretical extinction cross-sections. The initial concentration of the NP monomers was found to be 1.5×10^{-12} and 6.1×10^{-13} M for 58 and 78 nm diameter Ag NPs, respectively.

To make a comparison between the experimental spectrum and the spectra obtained after 27 min of adding 1 ng/mL IgG-Biot, it is necessary to know the fraction of dimers formed at this reaction time.

For the dimerization process

$$2M \rightarrow D$$

where M denotes Ag monomers and D denotes Ag NP dimers; the total concentration of particles (monomers plus dimers) $[NPs]_t$ at any time t can be expressed in terms of the initial concentration of NPs $[NPs]_i$ and the fraction of dimers $f_d = \frac{[D]_t}{[NPs]_t}$ as

$$[NPs]_t = [NPs]_i\left(\frac{1 - f_d}{1 + f_d}\right) + [NPs]_i\left(\frac{f_d}{1 + f_d}\right) \quad (1)$$

Therefore, the extinction at a given time t will be given by the following expression

$$E_t = [NPs]_i\left(\frac{1 - f_d}{1 + f_d}\right)\sigma_m + [NPs]_i\left(\frac{f_d}{1 + f_d}\right)\sigma_d \quad (2)$$

where E_t is the extinction at time t, σ_m is the extinction cross-section of the monomers, and σ_d is the extinction cross-section of the dimers. Note that the first and second terms in eq 2 correspond to the partial contribution to the extinction of monomers and dimers, respectively.

Using the above expression, together with the initial Ag NP concentrations as well as the theoretical cross-sections, the fraction of dimers f_d can be determined by varying its value in a systematic way until the theoretical peak intensity of the extinction spectra fits with the experimental one. Using this procedure, it was determined that f_d = 0.9 and f_d = 0.2 for the 58 and 78 nm diameter Ag NP dispersions, respectively (see red lines in Figure 5A,B).

Dividing eq 2 by the initial extinction, $E_0 = [NPs]_i\sigma_m$, the degree of depletion E_d is given by

$$E_d = \left(\frac{1 - f_d}{1 + f_d}\right) + [NPs]_i\left(\frac{f_d}{1 + f_d}\right)\left(\frac{\sigma_d}{\sigma_m}\right) \quad (3)$$

which indicates that E_d is determined by the ratio of the cross-section of the monomer and the corresponding dimer, for a given value of f_d. The variation of E_d with f_d is almost the same

DOI: 10.1021/acsomega.7b01840
ACS Omega 2018, 3, 2340−2350

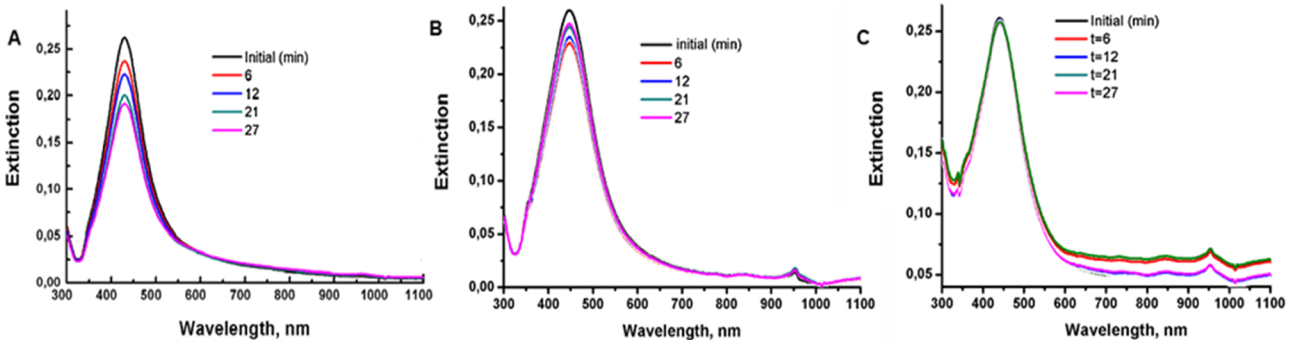

Figure 6. (A) Evolution of the extinction spectra of 58 nm diameter colloidal dispersion of Ag NPs previously functionalized with STV−Biot up to a time of 27 min after the addition of the antibody (with a final concentration of 1 ng/mL of IgG Biot). (B) Under the same conditions but in the presence of 5 pg/mL antigen. (C) Under the same conditions but in the presence of 15 pg/mL antigen.

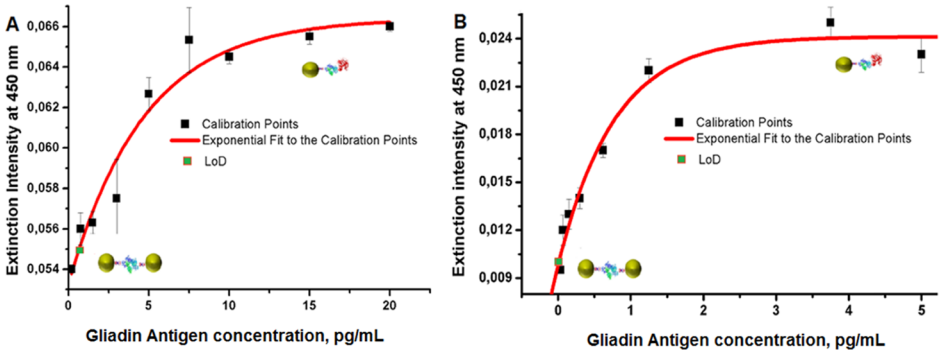

Figure 7. IDILA experimental calibration curve for gliadin antigen in the presence of 1 ng/mL gliadin specific biotinylated antibody for two different size colloidal dispersions of functionalized Ag NPs for (A) 58 and (B) 78 nm average diameters. The error was calculated as the average of three calibration curves. Both curves could be fitted to a function $I = I_0A_0 \exp(bc)$, where I is the extinction intensity and c is the antigen concentration. The parameters for the curve in panel A are $I_0 = 0.066$, $A_0 = 0.013$, and $b = 0.215$, whereas for the curve in panel B, they are $I_0 = 0.024$, $A_0 = 0.04$, and $b = 1.315$.

for Ag NP average diameters in the range of 48−68 nm, whereas it becomes significantly different for diameters around 78 nm (see Figure S7 and the respective discussion). Therefore, we considered it suitable to test the performance of the method for Ag NP sizes where σ_d/σ_m and hence the respective extinction depletion depicts quite different behavior, that is, for Ag NP average sizes around 58 and 78 nm.

Inhibition of Dimer Formation. The question that now arises is what happens if the antigen and the antibody are present simultaneously during the dimerization process. To address this issue, we compare the evolution of the extinction spectra of Biot−STV-functionalized 58 nm diameter Ag NPs at a constant Biot-IgG concentration (1 ng/mL) in the absence (Figure 6A) and presence of the antigen (gliadin) at two different concentrations (Figure 6B,C). Inhibition of the formation of dimers will be evidenced spectrally by a decrease in the degree of depletion of the extinction intensity. In the absence of the antigen, after the addition of 1 ng/mL Biot-Ig, the extinction spectra decreases, reaching maximum depletion after 27 min, indicating the formation of dimers (Figure 6A). The results obtained when the same experiment is carried out with the addition of 5 pg/mL antigen (Figure 6B) indicate that although there is a decrease in the intensity of the extinction spectrum, the value that reaches the intensity at the same time (27 min) is lower compared to the same assay performed without the presence of antibody (Figure 6A), indicating that the formation of dimers is less favored. In the presence of 15 pg/mL antigen (Figure 6C), no significant changes in the intensity of the extinction spectrum are observed; therefore, it seems that under this condition, the antigen concentration is high enough that the formation of dimers is totally inhibited.

These experiments clearly evidence that the optical response depends on the concentration of the antigen. This property is central because it will allow us in principle to build a calibration curve and the subsequent quantification of the antigen in the problem samples.

Building the Calibration Curve for Gliadin Detection by IDILA. To build the calibration curve, the IDILA assay was performed using Ag NPs of two different diameters (58 and 78 nm) at the same antibody concentration (1 ng/mL). The reason for choosing the same concentration of IgG-Biot and two different Ag NP diameters is to analyze if there is any influence of the fraction of dimers formed on the sensitivity and capability of the technique for gliadin detection. As discussed above, for 1 ng/mL antibody concentration, the fraction of dimers formed for 58 nm Ag NPs ($f_d = 0.9$) is significantly larger than for 78 nm Ag NPs ($f_d = 0.2$). The calibration curve was constructed by recording the extinction intensity at 450 nm after 27 min of adding the antibody in the presence of different concentrations of antigen. Figure 7A,B shows the results obtained for 58 and 78 nm diameter Ag NPs, respectively. Both calibration curves can be fitted quite accurately by an exponential function of the type $E = -A_0e^{-bc} + I_0$. This function describes quite well the behavior observed, that is, the inhibition of dimer formation at relatively small antigen concentrations, which is translated by an increase of the

DOI: 10.1021/acsomega.7b01840
ACS Omega 2018, 3, 2340−2350

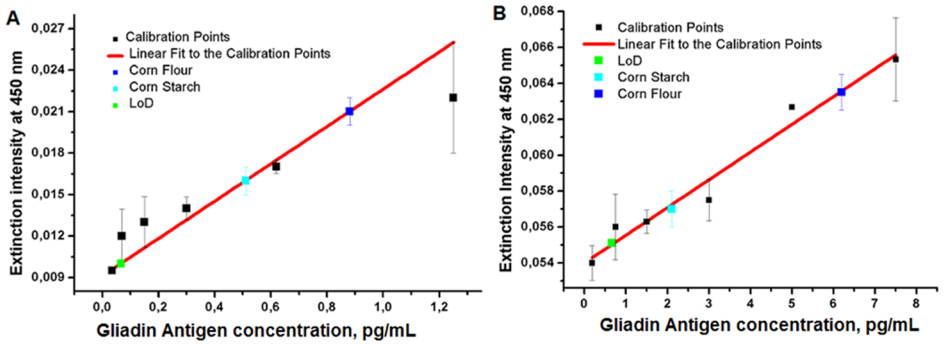

Figure 8. Linear fit of the IDILA calibration curve (taken from the corresponding exponential fits of Figure 7) for the quantification of samples of corn starch and corn flour. (A) In the range 0 1.2 pg/mL for the experiments performed with 78 nm diameter Ag NPs and (B) in the range 0 8 pg/mL for the experiments performed using 58 nm diameter Ag NPs. Standard deviations were taken as the average of three replicates for each problem sample.

extinction intensity and the almost total inhibition of the formation of dimers produced at larger antigen concentrations, which gives rise to an almost constant (no change) extinction intensity.

To assess the analytical performance of a quantification method, it is a standard practice to linearize the initial portion of the calibration curve. It was found that both curves could be fitted quite well by a linear expression in the range of 0−1.2 pg/mL for 78 nm diameter Ag NPs and 0−8 pg/mL for 58 nm diameter Ag NPs, as respectively depicted in Figure 8A,B. Comparing both calibration curves, the first difference that can be observed is that the linear range of quantification is larger for 58 nm Ag NPs than for 78 nm. This behavior could be explained considering that the fraction of dimers formed using 1 ng/mL antibody for 78 nm is smaller than for 58 nm Ag NPs (see simulations shown in Figure 5), therefore, a significant smaller antigen concentration (1.2 pg/mL) is needed to inhibit the formation of dimers. Another important difference between both calibration curves is the limit of detection (LOD), the limit of quantification (LOQ), and the sensitivity. The LOD and sensitivity of the technique are 20 times smaller and 6 times larger using 78 nm Ag NPs in comparison with the values obtained for 58 nm Ag NPs. This seems to be a contra-intuitive conclusion because for the experiments performed for 78 nm Ag NPs, the fraction of dimers formed is relatively smaller (f_d = 0.2) than for 58 nm Ag NPs (f_d = 0.9). However, it should be realized that if there is a smaller dimer fraction, then a small variation of the dimer concentration should be translated to a more significant change on the extinction intensity than when there is a larger dimer fraction (see eq 5 and Figure S7 and the respective discussion in the Supporting Information)

Gliadin Extraction and Detection in Food Samples. To test whether gliadin extraction from the food samples has been effective, we performed the western blot assay and Fourier transform infrared (FT-IR) spectroscopy with attenuated total reflectance (IR-ATR) characterization (see Figure S8).

The results obtained show that the method is effective in extracting the gliadin complex in oat and wheat food samples, whereas for corn flour and corn starch, neither of these techniques is sensitive enough to determine the presence of gliadin because corn has very low contents of gluten.

Therefore, to quantify the content of gliadin in these samples, a method with a very small LOD should be required. The IDILA or ELISA technique having a lower LOD seem to be, in principle, suitable for this purpose.

Gliadin Detection by ELISA. The ELISA calibration curve for gliadin detection was constructed using the methodology described in the Supporting Information (microplate reader measurements) and could be fitted quite accurately to a linear function with a mean square deviation of 0.97 (red line Figure 9). The LOD for gliadin using ELISA, calculated as the blank measured intensity plus 3 standard deviations, was found to be 1.82 ng/mL.

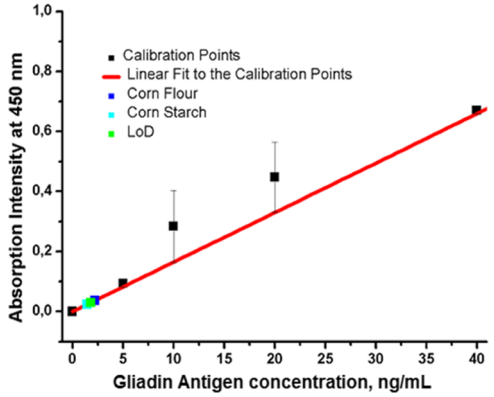

Figure 9. Calibration curve for gliadin using the ELISA method obtained from the commercially available kit. The LOD for gliadin was found to be 1.82 ng/mL. From this curve, the concentration of gliadin in real samples of corn starch was found to be below the LOD, whereas for corn flour, a value of 2.2 ± 0.1 ng/mL was determined.

The values of the amount of gliadin for the corn flour sample give a gliadin content of 2.2 ± 0.1 ng/mL, a value that is above the LOD. However, for the corn starch sample, the values obtained are below the LOD; hence, the amount of gliadin in these samples is not able to be quantified by ELISA.

Gliadin Detection by IDILA. As it has been shown above, the LOD of the IDILA technique is 0.52 pg/mL (for 58 nm Ag NPs) and 0.025 pg/mL (for 78 nm Ag NPs), values that are by far smaller than those obtained for the same antigen using ELISA. Therefore, it is expected that the IDILA technique should be able to quantify the amount of gliadin for both corn starch and corn flour. According to the Ag NP size employed (58 or 78 nm), to quantify the amount of gliadin, the problem samples were diluted 1000 and 10 000 times, respectively (because the LOQ of IDILA is almost 10 times smaller for 78 nm than for 58 nm Ag NPs)

DOI: 10.1021/acsomega.7b01840
ACS Omega 2018, 3, 2340−2350

The quantified values for gliadin in corn flour obtained from the linear fitting of the calibration curve for both Ag NP sizes (Figure 8A,B) are 6 ± 1 and 9.2 ± 0.6 pg/mL (multiplied by the corresponding dilution factor), values that are very close between them (within the experimental error) and also with the ELISA values (2.2 ng/mL, considering the dilution factor gives a value around 8 pg/mL). For the corn starch samples, the gliadin concentrations obtained are 2.0 ± 0.5 and 4.5 ± 0.2 pg/mL, again in fairly good agreement between them. An important aspect to consider is that the IDILA assay was able to quantify a small amount of gliadin in the corn starch samples (note that in this case, they were diluted by a factor of 1000−10 000 with respect to the ELISA samples) where the ELISA method failed because it is below its LOD.

Comparison between IDILA and ELISA. The comparison between the two assays can be analyzed in terms of two aspects. The first corresponds to the information related to the quantification of antigen in real samples. It should first be noted that IDILA is a technique that allows the detection of very low concentrations of antigen under study using dilution factors different from those used in the ELISA. Table 1 summarizes the results for the quantification of corn flour and corn starch in real samples. It can be appreciated that there is good agreement between the values obtained between both methodologies, considering that the corresponding dilution of the ELISA technique gives a final concentration of gliadin in the corn flour of 4.5 ± 0.7 mg/kg. On the other hand, the IDILA quantification of gliadin in the same sample of corn flour results in a concentration of 3 ± 1 mg/kg (using 58 nm Ag NPs) or 5 ± 1 mg/kg (employing 78 nm Ag NPs). For the corn starch sample, the ELISA method was not able to quantify the antigen, whereas the IDILA method gave a value as small as 0.1 ± 0.08 or 0.18 ± 0.06 mg/kg (using 58 or 78 nm Ag NPs, respectively).

Table 1. Comparison between the ELISA and the IDILA Assays for the Quantification of Gliadin in Real Samples Using 1 ng/mL Gliadin-Specific Antibody and Two Different Ag NP Sizes

quantification method	gliadin concentration in corn starch (mg/kg)	gliadin concentration in corn flour (mg/kg)
ELISA	N/D	4.5 ± 0.7
IDILA using Ag NPs of 58 nm diameter with 0.9 dimer fraction	0.1 ± 0.08	3 ± 1
IDILA using Ag NPs of 78 nm diameter with 0.2 dimer fraction	0.18 ± 0.06	5 ± 1

The second aspect is related to the analytical figures of merit of each technique obtained from the calibration curves (Table 2). As pointed out below, the LOD of the IDILA assay is several orders of magnitude lower than that of the ELISA method. The value of LOD of the IDILA method can further be improved using antibody concentrations where the fraction of dimers formed is less favored, as in the experiments performed using 78 nm Ag NPs, where the LOD was decreased by a factor of 20 just by performing the assay with an antigen concentration such that 20% of dimers are formed. The IDILA sensitivity is another parameter that has been demonstrated to increase almost 10 000 times with respect to the ELISA method, but there is less significant increase of it (a factor of 6) working under conditions where a smaller fraction of dimers is formed.

Table 2. Comparison between the Analytical Parameters of IDILA and ELISA

	IDILA (pg/mL)		
	Ag NPs 58 nm	Ag NPs 78 nm	ELISA (ng/mL)
sensitivity	$(1.5 \pm 0.1) \times 10^3$	$(9 \pm 1) \times 10^3$	$(1.6 \pm 0.1) \times 10^2$
LOD	0.52	0.025	1.82
LOQ	2.1	0.2	4.87

Concerning the LOQ, the values for the IDILA technique are (in the linear regime) 4000−40 000 (depending on the conditions that favor more or less the fraction of dimers) smaller than those of the ELISA method.

Therefore, these ultrasmall LOD and LOQ parameters implies that with an amount of the sample thousands of times smaller than that used by ELISA, the gliadin antigen could be detected by IDILA.

CONCLUSIONS

In this work, we have demonstrated the applicability of IDILA for the detection of ultralow concentrations of gliadin in real samples of corn flour and corn starch and compared the results with the standard ELISA method. The IDILA assay was found to be 1000−10 000 times more sensitive than the ELISA method, also having better performance in terms of the smaller LOD and LOQ.

It has been rationalized using electrodynamics simulations that, after adding a given amount of antibody, it is possible to quantify the degree of dimerization by fitting the experimental extinction intensity at a given time (from the initial NP concentration and the extinction cross-section of the Ag NP monomers and dimers in the colloidal dispersion).

The process of inhibition of dimer formation in the presence of antigen has been studied at antibody concentrations that favor the formation of a large fraction of dimers (for 58 nm diameter Ag NPs) or the formation of a relatively small fraction (for 78 nm diameter NPs). It was demonstrated that working under conditions where this fraction is small, the LOD and LOQ decrease almost an order of magnitude. Nevertheless, both NP sizes are able to detect gliadin at pg/mL concentrations. In addition, IDILA was able to quantify amounts of gliadin in corn starch samples that have concentrations smaller by an order of magnitude (in ppm) than the LOD of the standard ELISA method.

Another important feature of this technique is its feasibility, in terms of its relatively faster execution time of about 2 h including the preparation of antigen, antibody, and the respective dilutions of reagents, and also because the assay is performed in solution and does not require washing steps.

In addition, it makes use of the same materials necessary to carry out the ELISA technique, that is, a microplate reader and traditional 96-well microplates allowing to perform this test with instrumentation commonly used in biochemistry laboratories. The smaller amounts of antibody and antigen used, evidenced by the significant smaller LOD and LOQ of the IDILA method (in the femtomolar concentration regime), makes this method significantly cheaper than the ELISA method.

DOI: 10.1021/acsomega.7b01840
ACS Omega 2018, 3, 2340−2350

MATERIALS AND METHODS

Materials. The following reagents were used: $AgNO_3$ (Blaker—Sigma-Aldrich); sodium citrate (Anhedra); EZ-Link Biotin-HPDP (Pierce); STV (Invitrogen); primary rabbit polyclonal IgG antibody to gliadin (LSBio); secondary biotinylated antibody to wheat gliadin (LSBio), buffer saline phosphate; polysorbate 20 (Tween 20) (Sigma-Aldrich); NeutrAvidin (Thermo Scientific); sulfuric acid; sodium dodecyl sulfate (SDS) containing 12% polyacrylamide gel; PBS—0.05% Tween 20; carbonate−bicarbonate buffer pH 9.6 (Na_2CO_3 1.59 g, NaHCO 32.93 g, distilled water q.s. 1000 mL); blocking solution (BSA 4.00 g, PBS 100 mL); diluent solution (BSA, 1.00 g, PBS 100 mL); western blot run buffer (25 mM Tris; 190 mM glycine; 0.1% SDS at pH 8.3) (Bio-Rad); tris buffer saline Tween 20 (Bio-Rad) (50 mM Tris, 150 mM NaCl, 0.1% Tween 20).

Methods. *Synthesis and Characterization of Ag NPs.* The synthesis of the Ag NPs was performed by a slight modification of the Turkevich method based on the reduction of the metallic salt ($AgNO_3$) with sodium citrate that also fulfills the role of a surfactant.[38] Ag NPs having 58 and 78 nm diameters were manufactured by adding 1 mL of 0.01 M sodium citrate and 1 mL of 0.01 M silver nitrate to 150 mL of water under magnetic stirring and then heating the solution till the boiling point. After 15 minutes, a volume of 90 μL (45 μL) of 0.01 M ascorbic acid was added to this solution for obtaining 58 nm (78 nm) Ag NPs, till a yellow (yellow white) color was observed. The optical and morphological characterizations were performed using UV−visible absorption spectroscopy in the range of 300−1100 nm, TEM, and by comparing the experimental spectra with the electrodynamics modeling using the Mie's theory.[39] Using the experimental peak extinction intensities and the extinction cross-section determined theoretically with the Mie theory together with Beer's law, the concentrations obtained for the 58 nm diameter and 78 nm diameter Ag NPs were 1.5×10^{-12} and 6.1×10^{-13} M, respectively. The diameters of the particles were obtained from the TEM images.

Ag NP Functionalization. Ag NPs were functionalized with STV (Invitrogen) and biotin (Biot) (EZ-Link Biotin HPDP, Pierce). For the surface modification of NPs, the colloidal dispersion was incubated simultaneously with STV−Biot in a molar ratio 1:1:1 for 1 h at room temperature.

Gliadin Extraction from Food Samples. A solution of 60% alcohol in water was used for the extraction of gliadin from samples of maize flour and maize starch, according to the following procedure:

(1) Dried and ground samples (0.25 g) were weighed and transferred to 10 mL propylene tubes.
(2) 60% alcohol in water solution (10 mL) was added to the propylene tubes and then incubated for 1 h at room temperature with a rotary shaker at 45 revolutions per min.
(3) The tubes were centrifuged for 10 min at 2500*g* at room temperature. One mL of the supernatant was transferred using a clean micropipette to 1.5 mL Eppendorf tubes, which was centrifuged for 5 min at 2500*g* at room temperature.
(4) The supernatant, containing the soluble fraction of gluten of the sample, was transferred to 1.5 mL Eppendorf tubes using Pasteur pipettes.[40]

Western Blot. The presence of gliadin in food samples under study was confirmed by the western blot analysis.[41,42] Gliadin was extracted (by 60% alcohol extraction) from the bulk material as detailed above. Samples of gliadin proteins (40 mg) were fractionated through SDS-containing 12% polyacrylamide gels and then electrotransferred to nitrocellulose membranes for 1 h at 100 V in transfer buffer solution (25 mM Tris, 190 mM glycine, 20% methanol). Membranes were blocked in 5% BSA−PBS for 3 h at 37 °C and then incubated overnight at 4 °C in PBS−Tween 20 0.05% containing specific anti-gliadin mouse monoclonal primary antibodies (LifeSpan BioSciences Inc., Seattle, WA, USA, diluted 1/1000). The washed membranes were then incubated for 2 h at room temperature with secondary goat IRDye 680LT anti-mouse antibodies (1/25 000, LI-COR Bioscience, Lincoln, NE, USA) and washed, and immunodetection was performed using ODYSSEY infrared imaging system (LI-COR Bioscience).

Gliadin Quantification by ELISA. To validate the methodology proposed in the present work (IDILA), gliadin was analyzed in the different samples by ELISA, which is the analytical method currently homologated for gliadin detection in food samples by the Codex Alimentarius.[43,44] A commercially available gliadin detection ELISA assay (LifeSpan BioSicences Inc., Seattle, WA, USA) was used. In brief, 96-well microplates plates were coated with 5 μg/mL polyclonal rabbit anti-gliadin antibody in 50 mM carbonate−bicarbonate buffer pH 9.6 (100 μL/well) overnight at 4 °C and then blocked with 5% BSA−PBS (200 μL/well) for 3 h at room temperature. Sample serial dilutions (100 μL/well) were incubated for 2 h at room temperature. Biotinylated rabbit anti-mouse IgG was added (diluted 1/1000, 100 μL/well) and incubated for 1 h at 37 °C. The plates were washed, and STV−peroxidase was added and incubated for 30 min at room temperature. After the washes, the reaction was developed with TMB substrate reagent (BD OptEIA, BD Biosciences, San Jose, CA, USA), and absorbance was recorded at 450 nm in a microplate reader (Bio-Rad Inc., Hercules, CA, USA).

IR-ATR Spectroscopy. This technique was used as an alternative tool to test if the extraction of gliadin from the analyzed samples has been successful (corn flour and corn starch). The spectra were taken in the range of 800−1900 cm^{-1} with a Nicolet Nexus FTIR spectrometer with a Spectral ATR Golden Gate Mk II accessory with diamond crystal and reflection. The equipment was purged with dry air to remove the contribution of the water vapor, and the samples were allowed to evaporate on the reflectance glass for subsequent acquisition of the spectra.[45−48]

Extinction Measurements. The characterization by UV−vis spectroscopy was carried out by scanning in the 300−1100 nm range. The spectra were measured using a Shimazdu UV-1700 PharmaSpec spectrophotometer with a 1 cm quartz cell at room temperature.

TEM. TEM images were obtained using a JEM-JEOL 1120 EXII under an accelerating voltage of 80 kV. Samples were prepared by adding one drop (~30 μL) of the samples colloidal solution onto a holey carbon−formvar-coated copper TEM grid (100 mesh).

Dynamic Light Scattering (DLS). DLS is a technique that is generally used to determine the particle diameter in a solution or colloidal dispersion, based on the temporal fluctuations of the particle dispersion in solution and correlating these fluctuations with the hydrodynamic radius of the particles. The optical characterization of the different NPs and nanostructures was performed using a Delsa Nano 2.2

DOI: 10.1021/acsomega.7b01840
ACS Omega 2018, 3, 2340−2350

spectrophotometer with a 1 cm quartz cell at room temperature.

Computational Methods. The optical response of Ag NPs was calculated using the Mie theory and the generalized multiparticle Mie theory (GMM).[39,49] In all calculations performed in this work, the NPs were excited by a plane wave with an incidence pointing vector (propagation direction) normal to the surface. All calculations were performed for 58 and 78 nm diameter Ag NPs with an interparticle spacing of 20 nm. The average extinction cross-section (σ_{Ext}) was calculated by averaging the extinction cross-sections obtained by illuminating the dimer with polarizations around the x, y, and z axes. $\sigma_{Ext} = \frac{1}{3}\sigma_x + \frac{1}{3}\sigma_y + \frac{1}{3}\sigma_z$. In all simulations, we have used the dielectric function tabulated by Palik for Ag.

■ ASSOCIATED CONTENT

Supporting Information

The Supporting Information is available free of charge on the ACS Publications website at DOI: 10.1021/acsomega.7b01840.

Chemical structure of biotin HPDP, biotin (SH), and pyridine-2-thione, schematic representation of the functionalization of an Ag NP with biotin (SH) and pyridine-2-thione, scheme showing the formation of biotin−STV-functionalized Ag NPs, stability of the colloidal dispersion of 58 nm diameter Ag NPs functionalized with STV−Biot produced under stoichiometric control, TEM image of 58 nm diameter Ag NPs synthesized by Turkevich method after functionalization with biotin HPDP, stability of Ag NPs, some representative TEM images of the dimeric structures obtained for two different average NP diameters after the addition of 1 ng/mL IgG-Biot, theoretical modelling using the Mie theory and GMM theory for the cross-section of one monomer, two monomers, and one dimer for 58 and 78 nm diameter Ag NPs, variation of the degree of depletion on the dimer fraction for three representative NP diameters, western blot with antibodies specific for gliadin, wheat flour, oats, and maize, FT-IR ATR spectra for wheat flour, maize flour, oats, and corn starch, and microplate reader measurements (PDF)

■ AUTHOR INFORMATION

Corresponding Author

*E-mail: coronado@fcq.unc.edu.ar (E.A.C.).

ORCID

Eduardo A. Coronado: 0000-0002-0748-6803

Author Contributions

P.A.M. designed and performed the experiments, J.C.F. participated in the initial stage of this research, R.D.M. provided guidance and assistance regarding the immunology studies and performed the ELISA measurements, and E.A.C. designed the research, cowrote the manuscript, and provided overall guidance. P.A.M. is the main author of this work.

Notes

The authors declare no competing financial interest.

■ ACKNOWLEDGMENTS

The authors also acknowledge the financial support of CONICET (PIP 112-201101-00430), FONCYT (PICT 2012-2286, PICT 2012-3094, PICT 2014-2195), SECYT-UNC, and PME 1544-2006. P.A.M. acknowledges CONICET for being the recipient of a PhD fellowship.

■ REFERENCES

(1) Laube, T.; Kergaravat, S. V.; Fabiano, S. N.; Hernández, S. R.; Alegret, S.; Pividori, M. I. Magneto immunosensor for gliadin detection in gluten free foodstuff: Towards food safety for celiac patients. *Biosens. Bioelectron.* **2011**, *27*, 46−52.

(2) Araya Q, M. Mejorar el manejo de la enfermedad celíaca: Un desafío urgente. *Rev. Med. Chile* **2006**, *134*, 361−364.

(3) Fasano, A.; Berti, I.; Gerarduzzi, T.; Not, T.; Colletti, R. B.; Drago, S.; Elitsur, Y.; Green, P. H. R.; Guandalini, S.; Hill, I. D.; Pietzak, M.; Ventura, A.; Thorpe, M.; Kryszak, D.; Fornaroli, F.; Wasserman, S. S.; Murray, J. A.; Horvath, K. Prevalence of Celiac Disease in at risk and not at risk groups in the United States a large multicenter study. *Arch. Intern. Med.* **2003**, *163*, 286−292.

(4) Gujral, N.; Freeman, H. J.; Thomson, A. B. R. Celiac disease: prevalence, diagnosis, pathogenesis and treatment. *World J. Gastroenterol.* **2012**, *18*, 6036−6059.

(5) Koehler, P.; Schwalb, T.; Immer, U.; Lacorn, M.; Wehling, P.; Don, C. AACCI Approved Methods Technical Committee report: Collaborative study on the immunochemical determination of partially hydrolyzed gluten using an R5 competitive ELISA. *Cereal Foods World* **2013**, *58*, 154−158.

(6) Freedman, A. R.; Galfrè, G.; Gal, E.; Ellis, H. J.; Ciclitira, P. J. Monoclonal antibody ELISA to quantitate wheat gliadin contamination of gluten free foods. *J. Immunol. Methods* **1987**, *98*, 123−127.

(7) Baker, G. A.; Lajtha, S.; Dunn, H. A. *Handbook of Neurochemistry and Molecular Neurobiology: Practical Neurochemistry Methods*; Springer Science: New York, 2007; pp 193−219.

(8) Stephanie, D.; Gan, K.; Patel, K. R. Enzyme immunoassay and enzyme linked immunosorbent assay. *J. Invest. Dermatol.* **2013**, *133*, 1−3.

(9) Zhao, L.-J.; Yu, R.-J.; Ma, W.; Han, H.-X.; Tian, H.; Qian, R.-C.; Long, Y.-T. Sensitive detection of protein biomarkers using silver nanoparticles enhanced immunofluorescence assay. *Theranostics* **2017**, *7*, 876−883.

(10) Farka, Z.; Juřík, T.; Kovář, D.; Trnková, L.; Skládal, P. Nanoparticle based immunochemical biosensors and assays: recent advances and challenges. *Chem. Rev.* **2017**, *117*, 9973−10042.

(11) Aaron, J.; Travis, K.; Harrison, N.; Sokolov, K. Dynamic imaging of molecular assemblies in live cells based on nanoparticle plasmon resonance coupling. *Nano Lett.* **2009**, *9*, 3612−3618.

(12) De la Rica, R.; Stevens, M. M. Plasmonic ELISA for the ultrasensitive detection of disease biomarkers with the naked eye. *Nat. Nanotechnol.* **2012**, *7*, 821−824.

(13) Rodríguez-Lorenzo, L.; De la Rica, R.; Álvarez-Puebla, R. A.; Liz Marzán, L. M.; Stevens, M. M. Plasmonic nanosensors with inverse sensitivity by means of enzyme guided crystal growth. *Nat. Mater.* **2012**, *11*, 604−607.

(14) Mayilo, S.; Kloster, M. A.; Wunderlich, M.; Lutich, A.; Klar, T. A.; Nichtl, A.; Kürzinger, K.; Stefani, F. D.; Feldmann, J. Long range fluorescence quenching by gold nanoparticles in a Sandwich Immunoassay for cardiac troponin T. *Nano Lett.* **2009**, *9*, 4558−4563.

(15) Tang, S.; Hewlett, I. Nanoparticle Based immunoassays for sensitive and early detection of human immunodeficiency type 1 capsid (p24) antigen. *J. Infect. Dis.* **2010**, *201*, S59−S64.

(16) Wang, C.; Luconi, M.; Masi, A.; Fernandez, L. *Silver Nanoparticles as Optical Sensors, Silver Nanoparticles*; Pozo Perez, D., Ed.; InTechOpen, 2010; pp 225−255.

(17) Fraire, J. C.; Masseroni, M. L.; Jausoro, I.; Perassi, E. M.; Añel, A. M. D.; Coronado, E. A. Identification, localization, and quantification of neuronal cell membrane receptors with Plasmonic Probes: role of protein kinase D1 in their distribution. *ACS Nano* **2014**, *8*, 8942−8958.

(18) De la Rica, R.; Stevens, M. M. Plasmonic ELISA for the ultrasensitive detection of disease biomarkers with the naked eye. *Nat. Nanotechnol.* **2012**, *7*, 821−824.

DOI: 10.1021/acsomega.7b01840
ACS Omega 2018, 3, 2340−2350

(19) Yu, R.-J.; Ma, W.; Liu, X.-Y.; Jin, H.-Y.; Han, H.-X.; Wang, H.-Y.; Tian, H.; Long, Y.-T. Metal linked immunosorbent assay (MeLISA): the enzyme free alternative to ELISA for biomarker detection in serum. *Theranostics* **2016**, *6*, 1732−1739.
(20) Wang, Q.; Pan, M.; Wei, J.; Liu, X.; Wang, F. Evaluation of DNA Methyltransferase Activity and Inhibition via Isothermal Enzyme Free Concatenated Hybridization Chain Reaction. *ACS Sens.* **2017**, *2*, 932−939.
(21) Kelly, K. L.; Coronado, E.; Zhao, L. L.; Schatz, G. C. The optical properties of metal nanoparticles: the influence of size, shape, and dielectric environment. *J. Phys. Chem. B* **2003**, *107*, 668−677.
(22) Su, K.-H.; Wei, Q.-H.; Zhang, X.; Mock, J. J.; Smith, D. R.; Schultz, S. Interparticle coupling effects on plasmon resonances of nanogold particles. *Nano Lett.* **2003**, *3*, 1087−1090.
(23) Gunnarsson, L.; Bjerneld, E. J.; Xu, H.; Petronis, S.; Kasemo, B.; Käll, M. Interparticle coupling effects in nanofabricated substrates for surface-enhanced Raman scattering. *Appl. Phys. Lett.* **2001**, *78*, 802−804.
(24) Jain, P. K.; El-Sayed, M. A. Surface plasmon resonance sensitivity of metal nanostructures: physical basis and universal scaling in metal nanoshells. *J. Phys. Chem. C* **2008**, *112*, 4954−4960.
(25) Rechberger, W.; Hohenau, A.; Leitner, A.; Krenn, J. R.; Lamprecht, B.; Aussenegg, F. R. Optical properties of two interacting gold nanoparticles. *Opt. Commun.* **2003**, *220*, 137−141.
(26) Le Ru, E.; Etchegoin, P. G. *Principles of Surface Enhanced Raman Spectroscopy*; Elsevier Science: Amsterdam, 2008; Vol *1*.
(27) Fraire, J. C.; Masseroni, M. L.; Jausoro, I.; Perassi, E. M.; Añel, A. M. D.; Coronado, E. A. Identification, localization, and quantification of neuronal cell membrane receptors with plasmonic Probes: role of protein kinase D1 in their distribution. *ACS Nano* **2014**, *8*, 8942−8958.
(28) Sperling, R. A.; Parak, W. J. Surface modification, functionalization and bioconjugation of colloidal inorganic nanoparticles. *Philos. Trans. R. Soc., A* **2010**, *368*, 1333−1383.
(29) Sokolov, K.; Follen, M.; Aaron, J.; Pavlova, I.; Malpica, A.; Lotan, R.; Richartz Kortum, R. Real time vital optical imaging of precancer using anti epidermal growth factor receptor antibodies conjugated to gold nanoparticles. *Cancer Res.* **2003**, *63*, 1999−2004.
(30) El-Sayed, I. H.; Huang, X.; El-Sayed, M. A. Surface plasmon resonance scattering and absorption of anti EGFR antibody conjugated gold nanoparticles in cancer diagnostics: applications in oral cancer. *Nano Lett.* **2005**, *5*, 829−834.
(31) Sönnichsen, C.; Alivisatos, A. P. Gold nanorods as novel nonbleaching plasmonbased orientation sensors for polarized single particle microscopy. *Nano Lett.* **2005**, *5*, 301−304.
(32) Wang, H.; Huff, T. B.; Zweifel, D. A.; He, W.; Low, P. S.; Wei, A.; Cheng, J.-X. In vitro and in vivo two photon luminescence imaging of single gold nanorods. *Proc. Natl. Acad. Sci. U.S.A.* **2005**, *102*, 15752−15756.
(33) Yu, C.; Irudayaraj, J. Multiplex biosensor using gold nanorods. *Anal. Chem.* **2007**, *79*, 572−579.
(34) Murphy, C. J.; Gole, A. M.; Hunyadi, S. E.; Stone, J. W.; Sisco, P. N.; Alkilany, A.; Kinard, B. E.; Hankins, P. Chemical sensing and imaging with metallic nanorods. *Chem. Commun.* **2008**, 544−557.
(35) Fraire, J. C.; Pérez, L. A.; Coronado, E. A. Rational design of plasmonic nanostructures for biomolecular detection: interplay between theory and experiments. *ACS Nano* **2012**, *6*, 3441−3452.
(36) Fraire, J. C.; Pérez, L. A.; Coronado, E. A. Cluster size effects in the SERS response of Ag and Au nanoparticle aggregates: experimental and theoretical insight. *J. Phys. Chem. C* **2013**, *117*, 23090−23107.
(37) Fraire, J. C.; Motrich, R.; Coronado, E. A. Design of a novel plasmonic nanoconjugated analytical tool for ultrasensitive antigens quantification. *Nanoscale* **2016**, *8*, 17169−17180.
(38) Turkevich, J.; Stevenson, P. C.; Hillier, J. A study of the nucleation and growth processes in the synthesis of colloidal gold. *Discuss. Faraday Soc.* **1951**, *11*, 55−75.
(39) Mie, G. Beiträge zur Optik trüber Medien, speziell kolloidaler Metallösungen. *Ann. Phys* **1908**, *330*, 377−445.
(40) García, E.; Llorente, M.; Hernando, A.; Kieffer, R.; Wieser, H.; Méndez, E. Development of a general procedure for complete extraction of gliadins for heat processed and unheated foods. *Eur. J. Gastroenterol. Hepatol.* **2005**, *17*, 529−539.
(41) Sandiford, C. P.; Tatham, A. S.; Fido, R.; Welch, J. A.; Jones, M. G.; Tee, R. D.; Shewry, P. R.; Taylor, A. J. N. Identification of the major water/salt insoluble wheat proteins involved in cereal hypersensitivity. *Clin. Exp. Allergy* **1997**, *27*, 1120−1129.
(42) Freedman, A. R.; Galfre, G.; Gal, E.; Ellis, H. J.; Ciclitira, P. J. Western Immunoblotting of cereal proteins with monoclonal antibodies to wheat gliadin to investigate celiac disease. *Int. Arch. Allergy Immunol.* **1988**, *85*, 346−350.
(43) *Codex Alimentarius Commission Draft Revised Standard for Gluten Free Foods, Step 8*. ALINORM 08/31/26. 2008.
(44) Matsuo, H.; Kohno, K.; Morita, E. Molecular cloning, recombinant expression and IgE binding epitope of ω 5 gliadin, a major allergen in wheat dependent exercise induced anaphylaxis. *FEBS J.* **2005**, *272*, 4431−4438.
(45) Pézolet, M.; Bonenfant, S.; Dousseau, F.; Popineau, Y. Comparison between functional and solution states as determined by infrared spectroscopy. *FEBS Lett.* **1992**, *299*, 247−250.
(46) Popineau, Y.; Bonenfant, M.; Cornec, M.; Pezolet, M. A study by infrared spectroscopy of the conformations of gluten proteins differing in their gliadin and glutenin compositions. *J. Cereal Sci.* **1994**, *20*, 15−22.
(47) Secundo, F.; Guerrieri, N. ATR FT/IR Study on the interactions between gliadins and dextrin and their effects on protein secondary structure. *J. Agric. Food Chem.* **2005**, *53*, 1757−1764.
(48) Barth, A. Infrared spectroscopy of proteins. *Biochim. Biophys. Acta, Bioenerg.* **2007**, *1767*, 1073−1101.
(49) Myroshnychenko, V.; Rodríguez-Fernández, J.; Pastoriza-Santos, I.; Funston, A. M.; Novo, C.; Mulvaney, P.; Liz-Marzán, L. M.; De Abajo, J. G. Modelling the optical response of gold nanoparticles. *Chem. Soc. Rev.* **2008**, *37*, 1792−1805.

DOI: 10.1021/acsomega.7b01840
ACS Omega 2018, 3, 2340−2350